

Observation of the effect of gravity on the motion of antimatter


<https://doi.org/10.1038/s41586-023-06527-1>

Received: 6 May 2023

Accepted: 9 August 2023

Published online: 27 September 2023

Open access

 Check for updates

E. K. Anderson¹, C. J. Baker², W. Bertsche^{3,4}✉, N. M. Bhatt², G. Bonomi⁵, A. Capra⁶, I. Carli⁶, C. L. Cesar⁷, M. Charlton², A. Christensen⁸, R. Collister^{6,9}, A. Cridland Mathad², D. Duque Quiceno^{6,9}, S. Eriksson², A. Evans^{6,9}, N. Evetts⁹, S. Fabbri^{3,10}, J. Fajans⁸✉, A. Ferwerda¹¹, T. Friesen¹², M. C. Fujiwara⁶, D. R. Gill⁶, L. M. Golino², M. B. Gomes Gonçalves², P. Grandemange⁶, P. Granum¹, J. S. Hangst¹✉, M. E. Hayden¹³, D. Hodgkinson^{3,8}, E. D. Hunter⁸, C. A. Isaac², A. J. U. Jimenez⁶, M. A. Johnson^{3,4}, J. M. Jones², S. A. Jones¹⁴, S. Jonsell¹⁵, A. Khramov^{6,9,16}, N. Madsen², L. Martin⁶, N. Massacret⁶, D. Maxwell², J. T. K. McKenna^{1,3}, S. Menary¹¹, T. Momose^{6,9,17}, M. Mostamand^{6,17}, P. S. Mullan^{2,18}, J. Nauta², K. Olchanski⁶, A. N. Oliveira¹, J. Peszka^{2,18}, A. Powell¹², C. Ø. Rasmussen¹⁹, F. Robicheaux²⁰, R. L. Sacramento⁷, M. Sameed^{3,21}, E. Sarid^{22,23}, J. Schoonwater², D. M. Silveira⁷, J. Singh³, G. Smith^{6,9}, C. So⁶, S. Stracka²⁴, G. Stutter^{1,25}, T. D. Tharp²⁶, K. A. Thompson², R. I. Thompson^{6,12}, E. Thorpe-Woods², C. Torkzaban⁸, M. Urioni⁵, P. Woosaree¹² & J. S. Wurtele⁸

Einstein's general theory of relativity from 1915¹ remains the most successful description of gravitation. From the 1919 solar eclipse² to the observation of gravitational waves³, the theory has passed many crucial experimental tests. However, the evolving concepts of dark matter and dark energy illustrate that there is much to be learned about the gravitating content of the universe. Singularities in the general theory of relativity and the lack of a quantum theory of gravity suggest that our picture is incomplete. It is thus prudent to explore gravity in exotic physical systems. Antimatter was unknown to Einstein in 1915. Dirac's theory⁴ appeared in 1928; the positron was observed⁵ in 1932. There has since been much speculation about gravity and antimatter. The theoretical consensus is that any laboratory mass must be attracted⁶ by the Earth, although some authors have considered the cosmological consequences if antimatter should be repelled by matter^{7–10}. In the general theory of relativity, the weak equivalence principle (WEP) requires that all masses react identically to gravity, independent of their internal structure. Here we show that antihydrogen atoms, released from magnetic confinement in the ALPHA-g apparatus, behave in a way consistent with gravitational attraction to the Earth. Repulsive 'antigravity' is ruled out in this case. This experiment paves the way for precision studies of the magnitude of the gravitational acceleration between anti-atoms and the Earth to test the WEP.

The weak equivalence principle (WEP) has recently been tested for matter in Earth's orbit¹¹ with a precision of order 10^{-15} . Antimatter has hitherto resisted direct ballistic tests of the WEP due to the lack of a stable, electrically neutral, test particle. Electromagnetic forces on charged antiparticles make direct measurements in the Earth's gravitational field extremely challenging¹². The gravitational force on a proton at the Earth's surface is equivalent to that from an electric field of

about 10^{-7} V m⁻¹. The situation with magnetic fields is even more dire: a cryogenic antiproton¹³ at 10 K would experience gravity-level forces in a magnetic field of order 10^{-10} T. Controlling stray fields to this level to unmask gravity is daunting. Experiments have, however, shown that confined, oscillating, charged antimatter particles behave as expected when considered as clocks^{14–16} in a gravitational field. The abilities to produce¹⁷ and confine¹⁸ antihydrogen now allow us to employ stable,

¹Department of Physics and Astronomy, Aarhus University, Aarhus, Denmark. ²Department of Physics, Faculty of Science and Engineering, Swansea University, Swansea, UK. ³School of Physics and Astronomy, University of Manchester, Manchester, UK. ⁴Cockcroft Institute, Sci-Tech Daresbury, Warrington, UK. ⁵University of Brescia, Brescia and INFN Pavia, Pavia, Italy. ⁶TRIUMF, Vancouver, British Columbia, Canada. ⁷Instituto de Física, Universidade Federal do Rio de Janeiro, Rio de Janeiro, Brazil. ⁸Department of Physics, University of California at Berkeley, Berkeley, CA, USA. ⁹Department of Physics and Astronomy, University of British Columbia, Vancouver, British Columbia, Canada. ¹⁰Accelerator and Technology Sector, CERN, Geneva, Switzerland. ¹¹Department of Physics and Astronomy, York University, Toronto, Ontario, Canada. ¹²Department of Physics and Astronomy, University of Calgary, Calgary, Alberta, Canada. ¹³Department of Physics, Simon Fraser University, Burnaby, British Columbia, Canada. ¹⁴Van Swinderen Institute for Particle Physics and Gravity, University of Groningen, Groningen, The Netherlands. ¹⁵Department of Physics, Stockholm University, Stockholm, Sweden. ¹⁶Department of Physics, British Columbia Institute of Technology, Burnaby, British Columbia, Canada. ¹⁷Department of Chemistry, University of British Columbia, Vancouver, British Columbia, Canada. ¹⁸Institute for Particle Physics and Astrophysics, ETH, Zurich, Switzerland. ¹⁹Experimental Physics Department, CERN, Geneva, Switzerland. ²⁰Department of Physics and Astronomy, Purdue University, West Lafayette, IN, USA. ²¹Accelerator Systems Department, CERN, Geneva, Switzerland. ²²Soreq NRC, Yavne, Israel. ²³Department of Physics, Ben Gurion University, Beer Sheva, Israel. ²⁴INFN Pisa, Pisa, Italy. ²⁵School of Mathematical and Physical Sciences, University of Sussex, Brighton, UK. ²⁶Physics Department, Marquette University, Milwaukee, WI, USA. ✉e-mail: william.bertsche@cern.ch; joel@physics.berkeley.edu; jeffrey.hangst@cern.ch

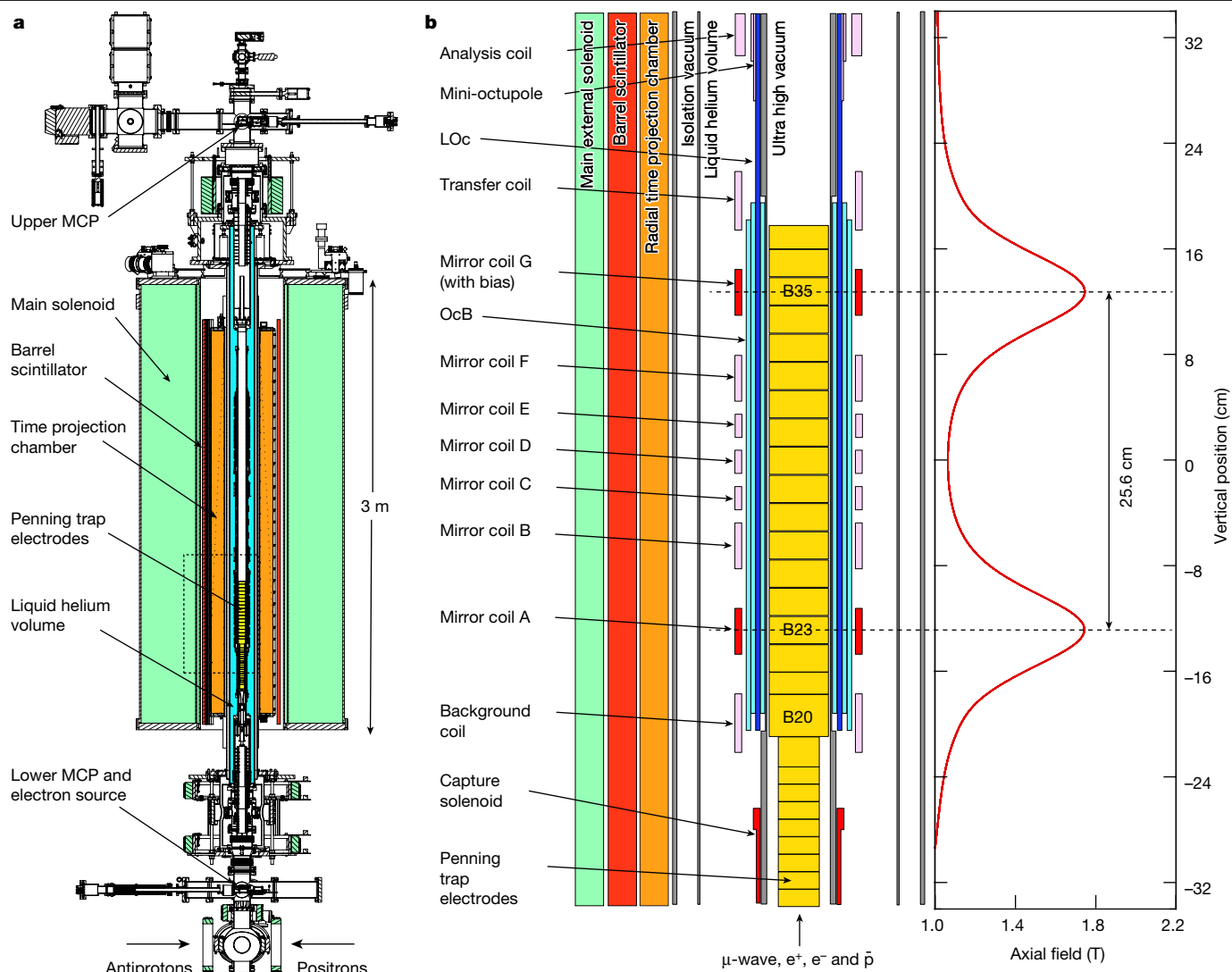


Fig. 1 | ALPHA-g apparatus. a, Cross section of the ALPHA-g apparatus. The full device comprises three antihydrogen trapping regions; only the bottom one is employed here. The MCP detectors are used to image charged particles (e^- , e^+ , \bar{p}) extracted from the Penning traps for diagnostic purposes. **b**, Expanded view of the bottom antihydrogen trap (the dashed rectangle in **a**) illustrating the Penning trap for antihydrogen production and the superconducting coils that form the neutral atom trap. The on-axis, axial field profile at full current is shown on the right. Note that the rTPC, the barrel scintillator and the

main solenoid are not drawn to scale here; see Fig. 1a for a scaled image. The mirror coils B–F, the analysis coil, the mini-octupole, the transfer coil and the background coil are not utilized here. The capture solenoid is used for charged particle transfer and manipulations and is de-energized for gravity measurements. The LOc coils (dark blue in the figure) extend past the trapping region used here and constitute part of two additional antihydrogen traps intended for future use.

neutral anti-atoms in dynamic experiments where gravity should play a role. Early considerations^{19,20} and a more recent proof-of-principle experiment²¹ in 2013 illustrated this potential. We describe here the initial results of a purpose-built experiment designed to observe the direction and the magnitude of the gravitational force on neutral antimatter.

Antihydrogen and ALPHA-g

Trapping and accumulation²² of antihydrogen are now routine, with up to several thousand atoms having been simultaneously stored in the ALPHA-2 device²³. To date, all of the measurements of the properties of antihydrogen^{24–29} have been performed in ALPHA magnetic traps. In 2018, the ALPHA-g machine—a vertically oriented antihydrogen trap designed to study gravitation—was constructed. The experimental strategy is conceptually simple: trap and accumulate atoms of antihydrogen; slowly release them by opening the top and bottom barrier potentials of the vertical trap; and try to discern any influence of gravity

on their motion when they escape and annihilate on the material walls of the apparatus. The trapped anti-atoms are not created at rest but have a distribution of kinetic energies consistent with the trap depth of about 0.5 K (we employ temperature-equivalent energy units). Gravity is expected to be manifested as a difference in the number of annihilation events from anti-atoms escaping via the top or the bottom of the trap.

The experimental layout is shown in Fig. 1. Antiprotons from the CERN Antiproton Decelerator³⁰ and the ELENA (Extra Low Energy Antiproton)³¹ ring are first caught in a separate, high voltage Penning trap in a 3 T solenoid magnet (not shown). ELENA typically delivers 7.5×10^6 antiprotons at 100 keV every 120 s. About 5×10^5 of these are dynamically captured. After being cooled by co-trapped electrons, antiprotons are injected into ALPHA-g and dynamically re-trapped. A superconducting solenoid provides the background field of 1 T for confining the charged particles. Positrons from a Surko-type accumulator³² are also injected into ALPHA-g and re-trapped; there are typically 3×10^6 available for each mixing cycle with antiprotons. The beamline

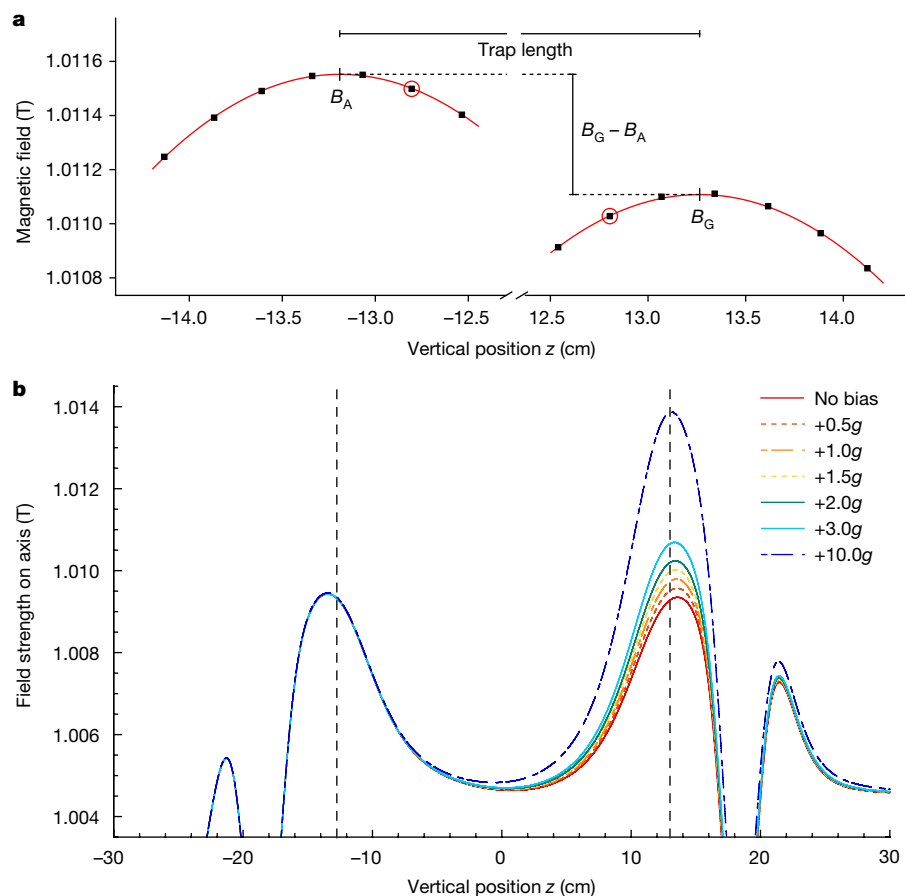


Fig. 2 | Illustrations of the magnetic bias. **a**, Expanded view of the end-of-ramp mirror coil peak regions for a bias of $-1g$ (note the discontinuous abscissa). The square points represent offline ECR measurements carried out to determine the field profile and to find the peak field location. The points with red circles indicate the axial locations at which ECR measurements were made at the

beginning and end of the mirror coil ramp-down for each gravity trial. **b**, Calculated on-axis final well shapes (after ramp-down) for the positive bias trials. The features at $|z| > 20$ cm are due to the OcB (Fig. 1) end turn windings. The vertical dashed lines represent the physical axial midpoints of mirrors A and G.

for guiding the bunches of positrons and antiprotons into ALPHA-g is described elsewhere³³. Following manipulations to control their size and density³⁴, the positron plasmas are mixed with antiproton plasmas in a region (electrodes B23 to B35 in Fig. 1) situated within the superconducting antihydrogen trap. The anti-atom trap comprises octupole magnets for transverse confinement and two solenoidal ‘mirror coils’ (A and G in Fig. 1) for axial (vertical) confinement. Antihydrogen atoms produced with sufficiently low kinetic energy can be trapped due to the $-\mu \cdot B$ interaction of their magnetic moments with the external fields. For the field strengths in ALPHA-g, the anti-atoms are spin-polarized, and the scalar magnitude of the magnetic field determines the trapping potential. The entire production and trapping region is cooled to near 4 K by the liquid helium bath for the trap magnets. ALPHA-g currently traps a few antihydrogen atoms per mixing cycle, but antihydrogen atoms can be accumulated²² over many cycles from ELENA. We refer to this process as ‘stacking’. The atom trapping volume is nominally a vertical cylinder of 4.4 cm diameter and 25.6 cm height.

The effect of gravity

The experimental protocol was to stack antihydrogen atoms, then release them by ramping down the current in the two mirror coils simultaneously over 20 s. The anti-atoms could escape either to the top of the trap (through mirror G) or the bottom (through mirror A) and subsequently annihilate on the walls of the apparatus (Fig. 1). The annihilations and their positions (vertices) could be detected and reconstructed using the ALPHA-g radial time projection chamber (rTPC) detector

(Fig. 1 and Methods). A coaxial, barrel-shaped scintillator detector was also used for event selection (Fig. 1 and Methods).

Numerical simulations of atom trajectories (Methods) indicate that if hydrogen atoms were trapped and gradually released from a vertically symmetric trap (that is, the on-axis magnetic field maxima are equal; $B_A = B_G$) under ALPHA-g conditions, about 80% of them would exit through the bottom, the asymmetry being due to the downward force of gravity. The goal of the current experiment was to test this behaviour for antihydrogen. Vertical gradients in the magnetic field magnitude can obviously mimic the effect of gravity. Quantitatively, the local acceleration of gravity g , which is about 9.81 m s^{-2} , is equivalent to a vertical magnetic field gradient of $1.77 \times 10^{-3} \text{ T m}^{-1}$ acting on a hydrogen atom in the ground state. The peaks in the mirror coil axial field strength are separated by 25.6 cm at full current, so a field difference of $4.53 \times 10^{-4} \text{ T}$ between these points would mimic gravity. This consideration sets the scale for the required degree of magnetic field control for this experiment, but it also allows us to refine the simple, symmetric release procedure to more systematically probe gravity. In particular, it is possible to either counteract or supplement gravity by introducing a differential current to one of the mirror coils.

We first consider a simplified, one-dimensional on-axis model. As the mirror fields are ramped down, a particular anti-atom will escape when its axial kinetic energy exceeds the combined gravitational and magnetic potential at the peak axial field position of one of the mirror coils. Thus, one could balance the effect of gravity on matter by imposing a field difference ($B_G - B_A$) of about $-4.53 \times 10^{-4} \text{ T}$ between the mirror field peaks (Fig. 2a). Maintaining this difference during the

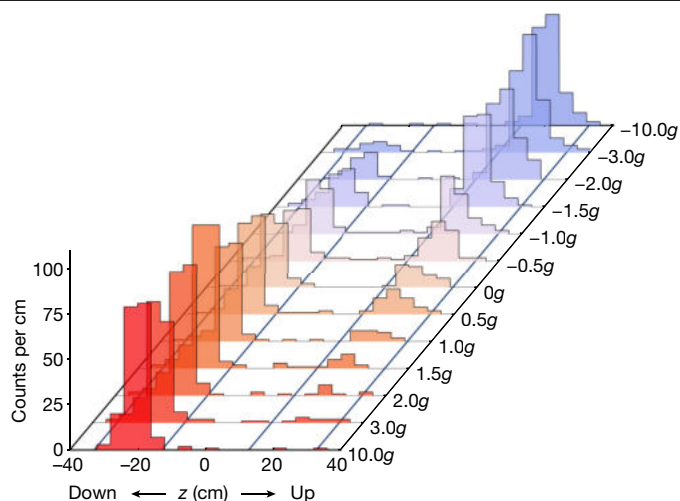


Fig. 3 | Escape histograms. The raw event z -distributions are displayed as histograms for each of the bias values, including the $\pm 10g$ calibration runs. These are uncorrected for background or detector relative efficiency. The time window represented here is 10 s to 20 s of the magnet ramp-down. The z -cut regions are indicated by the solid, diagonal lines. Explicitly, the acceptance regions in z are $[-32.8, -12.8]$ and $[12.8, 32.8]$ cm for the ‘down’ and ‘up’ regions, respectively.

ramp-down would in principle result in half of the atoms escaping in each direction. Note that this incremental field is very small compared to the size of the initial peak end field, which is about 1.74 T. The mirror coils A and G were connected in series, and a bipolar current supply connected only to mirror G could provide a field increment or decrement (Methods). We emphasize that a magnetic gradient is not applied uniformly over the length of the trap. The local field geometry in the region of each mirror coil determines which particles can escape axially.

The release experiment

In anticipation of future precision experiments, the octupole fields in ALPHA-g can be generated by three distinct coils. Two of these, which we designate long octupole (LOc) and bottom octupole (OcB), are employed here (Fig. 1). The OcB magnet (made up of six wound current layers) spans the axial trapping region employed in the current experiment. The LOc magnet comprises two layers of windings and extends over 1.5 m of the apparatus, covering two additional antihydrogen trapping regions not utilized here. For trapping and stacking, both octupole magnets are energized to about 830 A. At the completion of stacking, the LOc magnet is ramped down in 1 s, thereby eliminating the transverse confinement field above mirror G (Fig. 1). This step releases some of the more transversely energetic atoms – about half of the stacked sample. By counting the resulting annihilations, we obtain an indication of the total number of atoms that have been stacked.

The actual experiment involved many trials of antihydrogen accumulation and release for various magnetic ‘bias’ levels. We define the imposed bias as:

$$\frac{\mu_B(B_G - B_A)}{m_H(z_G - z_A)}$$

where μ_B is the Bohr magneton, $(B_G - B_A)$ is the difference between the on-axis field maxima under the two mirror coils, m_H is the hydrogen gravitational mass and $(z_G - z_A)$ is the height difference between the positions of the on-axis field maxima. It is convenient to express the bias relative to g . Thus, in the one-dimensional model, a magnetic bias of $-1g$ would effectively balance the downwards gravitational force for hydrogen. Having assumed no a priori direction or magnitude for the

gravitational force on antihydrogen, we investigated nominal bias values of $\pm 3g, \pm 2g, \pm 1.5g, \pm 1g, \pm 0.5g$ and $0g$. Figure 2b illustrates the positive bias fields ($B_G > B_A$), which would encourage antihydrogen atoms to exit at the bottom.

We typically accumulated anti-atoms for 50 stacks in roughly four hours, resulting in about 100 atoms trapped. For each trial, after the conclusion of stacking and the LOc ramp-down, the on-axis field magnitude at one axial location under each mirror coil (Fig. 2a) was measured using the technique of electron cyclotron resonance (ECR)³⁵ (Methods). The ECR measurement was made at approximately 130 s after the LOc ramp-down. The mirror coil current ramp-downs happened next and were linear over 20 s. The smaller of the two mirror fields was not ramped all the way down to the level of the bottom of the confinement well but stopped at about 5×10^{-3} T above this level. This was to ensure that the released atoms possessed enough energy to overcome the small axial field bumps that arise from the end windings of the OcB magnet (Fig. 2b). At approximately 96 s after the mirror ramp-down, the ECR measurements were repeated to characterize the final axial well (Methods).

Various bias values were interleaved during the data-taking period, which lasted about 30 days. We emphasize that the integer or half-integer bias values identified above are just labels for the trials and refer to the programmed on-axis field maxima; neither is the bias perfectly constant during the ramp-down, nor does the one-dimensional model completely characterize the three-dimensional experiment. Trials for a given bias were repeated six or seven times, depending on the total number of events detected. The raw results (no background subtraction or detector efficiency correction) are presented as axial annihilation distributions in Fig. 3. For further analysis, we exclude events whose z -position lies between the physical mirror centres, or more than 0.2 m outside the physical mirror centres, as indicated in Fig. 3. This ‘ z -cut’ was chosen by conducting a separate set of experiments in which we attempted to release trapped antihydrogen atoms to only the top or the bottom of the trap by applying a bias of $-10g$ or $+10g$, respectively. The $\pm 10g$ trials also help to determine the relative efficiency of the rTPC detector for the up and down escape regions (Methods). The efficiency determination uses the number of atoms detected in the LOc ramp-down as a normalization. The plotted event distributions were also subject to a ‘time cut’: events are accepted from 10 to 20 s of the ramp-down, as we found that the number of atoms emerging before 10 s is negligible (Fig. 4).

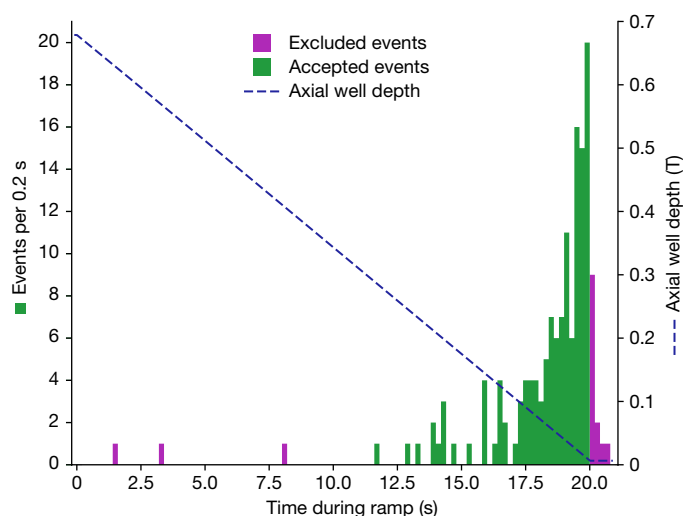


Fig. 4 | Time structure of the annihilation events from escaped antihydrogen. The number of detected events (left ordinate) is plotted as a function of time as the magnets are ramped down. This figure represents the sum of the seven trials having bias $0g$. The dashed line (right ordinate) illustrates the calculated axial well depth during the magnet ramp-down. The excluded events fail the time cut.

Table 1 | Results of the release trials

Nominal bias (g)	Number of trials	N_{up} (events)	N_{dn} (events)	Events during LOc ramp-down
-3.0	7	151.7	16.5	199.2
-2.0	7	128.7	33.5	168.2
-1.5	6	128.9	57.7	192.0
-1.0	7	69.7	62.5	183.2
-0.5	7	55.7	67.5	201.2
0	7	36.7	94.5	144.2
0.5	7	36.7	124.5	177.2
1.0	7	17.7	119.5	185.2
1.5	6	13.9	180.7	234.0
2.0	7	6.7	163.5	228.2
3.0	7	7.7	147.5	199.2
-10.0	6	142.9	0.7	169.0
10.0	6	-0.1	185.7	213.0

The number of events for anti-atoms escaping either up or down is tabulated for each bias series. These events occur in the time window 10–20 s during the ramp-down and lie within the z-regions illustrated in Fig. 3. Also shown is the number of events due to antihydrogen atoms that escape when the long octupole magnet is ramped down. All values are corrected for the expected cosmic ray background. Counting uncertainties are not listed but are used in the global determination of P_{dn} in Fig. 5. The background per trial was 0.18 ± 0.01 events in the top region and 0.21 ± 0.01 events in the bottom region. The background per trial for the LOc ramp-down window (duration 13.1 s) was 0.83 ± 0.02 events. The $\pm 10\text{g}$ entries are for the calibration trials (see text).

The essential cumulative result for each bias can be represented by two numbers, N_{up} and N_{dn} : the number of particles escaping upwards or downwards. These are listed in Table 1. The techniques used to maximize the signal and suppress the background are described in Methods. The background rates are listed in the Table 1 notes.

The escape curve

In Fig. 5 we plot the probability for an antihydrogen atom to escape downwards (P_{dn}) as a function of the applied bias. The probabilities and their credible intervals were obtained from the raw event counts by using standard statistical techniques (Methods). The biases plotted here are derived values, as the magnetic field difference (on axis) between the upper and lower barriers remains only approximately

constant as the current is decreased. This is due to small asymmetries in the background field, the construction of the mirror coils and the ramp-induced persistent currents in the superconductors (Methods). We also observe that these currents decay after the end of the ramp (Extended Data Fig. 6), affecting the final-well ECR measurements. To account for these effects, we use a measurement-based magnetic field model (Methods) to calculate the bias during the ramp. We can then assign to each annihilation event the calculated bias for the time at which that particular anti-atom escaped the trap (Fig. 4 and Extended Data Fig. 8). Finally, we average the biases for all of the events that pass our selection criteria (or ‘cuts’) to arrive at the plotted bias value for the collection of trials sharing the same magnetic field configuration. The uncertainties in the bias determination are of order 0.1g and are described in detail in Methods.

Qualitatively, the experimental data in Fig. 5 exhibit the behaviour characteristic of gravitational attraction between antihydrogen and the Earth. At a bias of about $+3\text{g}$ (-3g) the anti-atoms exit predominantly at the bottom(top) of the trap, as the magnetic imbalance is significantly larger than 1g . The fraction exiting through the bottom increases monotonically as the bias increases from -3g to $+3\text{g}$. The balance point ($P_{\text{dn}} = 0.5$) is close to -1g , as naively expected from the simplified one-dimensional argument presented above.

To gain more quantitative insight into the results (and originally to inform the design of the experiment) we rely on extensive numerical simulations (Methods) of the trajectories of antihydrogen atoms trapped and then released. The numerical model features a three-dimensional magnetic field map based on both the as-built superconducting magnet wire model and the measured fields from ECR or a magnetron frequency measurement technique (Methods). The actual currents measured during the experimental sequence are used for the simulation. This is the same magnetic field model used to derive the plotted biases above, so the simulation describes a three-dimensional system that is consistent with our best experimental measurements—both static and dynamic—of on-axis field strengths. The ECR measurements taken during the trials have been supplemented by extensive offline studies using both ECR and the magnetron method (Methods). The simulated release results are plotted with the data in Fig. 5, both for attractive (normal) gravity and, by way of comparison, for ‘no’ gravity and for ‘repulsive’ gravity.

The agreement between the shape of the measured data and that of the simulation is visually compelling. To extract a value for the local acceleration from our dataset, we have compared the data to a set of simulations that presume values for antihydrogen’s gravitational

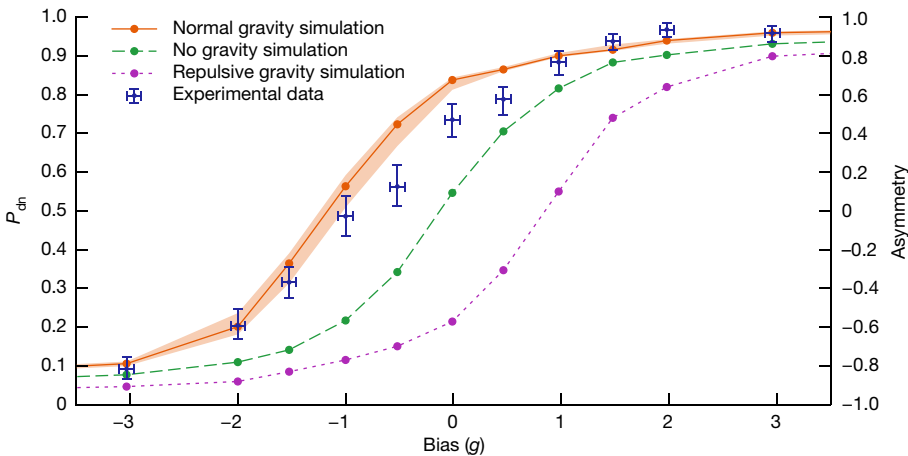


Fig. 5 | Escape curve and simulations. The derived P_{dn} values are plotted versus bias for the experimental data and for simulations of the experiment for three values of the gravitational acceleration a_g : 1g (normal gravity, orange), 0g (no gravity, green) and -1g (repulsive gravity, violet). See the text for the definitions

of the uncertainties. The right ordinate is the down-up asymmetry $A = 2P_{\text{dn}} - 1$. The confidence intervals on the no- and repulsive gravity simulations are comparable to those for the normal gravity simulation and have been omitted for clarity.

Table 2 | Uncertainties in the bias determination

Uncertainty	Magnitude (g)
ECR spectrum width	0.07
Repeatability of ($B_G - B_A$)	0.014
Peak field size and z-location fit	0.009
Field decay asymmetry (A to G) after ramp	0.02
Bias variation in time	0.02
Field modelling	0.05
Summary of the uncertainties in the derived bias values, expressed in units of the local acceleration of gravity for matter (9.81 m s^{-2}). See Methods for definitions and details.	

acceleration that differ from $1g$ (Extended Data Fig. 1). Generally speaking, the simulated curves have the same shape and are shifted along the bias axis. From a likelihood analysis (Methods) on the experimental data, we find that the local gravitational acceleration of antihydrogen is directed towards the Earth and has magnitude $a_g = (0.75 \pm 0.13 \text{ (statistical + systematic)} \pm 0.16 \text{ (simulation)})g$, where $g = 9.81 \text{ m s}^{-2}$. Within the stated errors, this value is consistent with a downward gravitational acceleration of $1g$ for antihydrogen.

Classification of uncertainties

Broadly speaking, we characterize three different types of uncertainty. The uncertainties regarding magnetic field measurement and modelling affect the derived bias values and are listed in Table 2 and described in Methods. These are reflected in the horizontal error bars on the bias values in Fig. 5. Statistical and systematic uncertainties regarding event detection, such as counting statistics, backgrounds and detector efficiencies, are listed in Table 3. These are manifested as vertical error bars in the P_{dn} values in Fig. 5. Finally, an estimated uncertainty band (orange band in Fig. 5) is associated with the simulation. This includes the potential impact of various unmeasured quantities, such as magnet winding misalignments, off-axis persistent magnetic fields, and uncertainty in the energy distributions (longitudinal and transverse) of the trapped antihydrogen atoms. All of the above are used to extract the uncertainties in the quoted value of a_g . Our goal here is not to make a precision determination of the magnitude of a_g , but to identify the statistical sensitivities and systematic effects that will be important for future measurements.

As a cross check, we conducted trials in which we used a 130 s ramp-down time, for biases of $0g$, $-1g$ and $-2g$. Within the calculated uncertainties, the results were consistent with the 20 s data and with the appropriate simulation (Extended Data Fig. 2).

We also observe that some atoms are released after the end of the 20 s ramp (Fig. 4 and Extended Data Fig. 3). This is potentially due to long-time-scale mixing³⁶ between the transverse and longitudinal motions of the atoms, but this has not yet been investigated in detail. The gravitational behaviour of these atoms appears to be consistent with the 20 s ramp-down sample (Extended Data Fig. 3), but the detailed systematic measurements to confirm this have not yet been performed.

Possible complicating effects

We have considered other effects that could mimic a gravitational force or add significant uncertainty, and we can rule them out due to their negligible magnitudes. We have earlier determined an experimental limit for the antihydrogen charge³⁷ to be less than about 10^{-28} C . Thus, a 1 V potential change would have the same effect as a 10^{-5} T change in magnetic field. The trap electrodes are maintained at their common ground to within $\pm 10 \text{ mV}$ after stacking is completed, so even the extremely unlikely presence of the maximal non-zero charge on

Table 3 | Uncertainties in the determination of a_g

	Uncertainty	Magnitude (g)
Statistical and systematic	Finite data size	0.06
	Calibration of the detector efficiencies in the up and down regions	0.12
	Other minor sources	0.01
Simulation model	Modelling of the magnetic fields (on-axis and off-axis)	0.16
	Antihydrogen initial energy distribution	0.03
Summary of the uncertainties involved in the determination of the gravitational acceleration a_g . The uncertainties are one standard deviation and are expressed in units of the local acceleration of gravity for matter (9.81 m s^{-2}). See Methods for the details.		

antihydrogen would play no role here. Concerning the size of the magnetic dipole moment of antihydrogen, we earlier measured the microwave transition²⁵ within the hyperfine-split ground state at approximately 1 T with an absolute accuracy corresponding to 0.3 mT. Since the positron magnetic dipole moment mainly determines the transition frequency, this corresponds to an uncertainty of the magnetic dipole moment of less than 1 part per thousand in antihydrogen, leading to a negligible contribution to the error budget here.

The measured masses and charges of the positron and antiproton³⁸ can, in the absence of new physics, be used to constrain the polarizability of an antihydrogen atom in the ground state to approximately that of the hydrogen ground state³⁹: $7.4 \times 10^{-41} \text{ C}^2 (\text{J m})^{-1}$. Thus, a change in electric field of 100 V m^{-1} would have an effect equivalent to a change in magnetic field of less than 10^{-13} T . Finally, antihydrogen atoms may change their velocity due to collisions with background gas during the ramp-down. From the measured antiproton storage lifetime of 4,000 s in the trap, we estimate the density of background gas to be approximately $2 \times 10^5 \text{ cm}^{-3}$. Using this value together with the calculated cross sections⁴⁰, the probability for a collision during the 20 s (130 s) ramp-down is less than 0.5% (3%).

Conclusion

We have searched for evidence of the effect of gravity on the motion of particles of neutral antimatter. The best fit to our measurements yields a value of $(0.75 \pm 0.13 \text{ (statistical + systematic)} \pm 0.16 \text{ (simulation)})g$ for the local acceleration of antimatter towards the Earth. We conclude that the dynamic behaviour of antihydrogen atoms is consistent with the existence of an attractive gravitational force between these atoms and the Earth. From the asymptotic form of the distribution of the likelihood ratio as a function of the presumed acceleration, we estimate a probability of 2.9×10^{-4} that a result, at least as extreme as that observed here, could occur under the assumption that gravity does not act on antihydrogen. The probability that our data are consistent with the repulsive gravity simulation is so small as to be quantitatively meaningless (less than 10^{-15}). Consequently, we can rule out the existence of repulsive gravity of magnitude $1g$ between the Earth and antimatter. The results are thus far in conformity with the predictions of General Relativity. Our results do not support cosmological models relying on repulsive matter–antimatter gravitation.

Future perspectives

This experiment marks the beginning of detailed, direct inquiries into the gravitational nature of antimatter. Having determined the sign and approximate magnitude of the acceleration, our next challenge is to extend the method to measure the magnitude as precisely as possible, to provide a more stringent test of the WEP. Colder atoms will obviously allow for more sensitive measurements, and our simulations indicate

that using colder antihydrogen atoms will in general steepen the transition region of the escape curve and allow for higher precision. Our recent demonstration of laser cooling of trapped antihydrogen²³ is a promising development in this direction. Additionally, our future measurements will incorporate adiabatic expansion cooling of trapped antihydrogen⁴¹. In addition to future measurements in ALPHA-g, alternative approaches are being pursued by the GBAR⁴² and AEGIS⁴³ collaborations at CERN.

The dependence on simulations is not a concern at the current level of precision, but supplementary experiments to benchmark and refine the simulations will form a large part of the future measurement programme. Our experimental technique is ultimately limited by the precision of the control and measurement of the magnetic fields in the atom trap and its surroundings. Offline magnetometry using electrons, nuclear magnetic resonance⁴⁴ (NMR) probes, and possibly trapped, laser cooled ions⁴⁵, will lead to refinement of the current method. The central trapping region of ALPHA-g, not yet utilized, is designed to be less susceptible to unprogrammed magnetic fields and to work with colder atoms. Having a cold source of stable antimatter in a vertical trap suggests the possibility of performing fountain-type, gravitational interferometry measurements⁴⁶, promising precisions of order 10^{-6} in the determination of a_g . Formerly the subject of countless thought experiments and indirect inferences, the motion of antimatter in the gravitational field of the Earth finally has a sound and promising experimental foothold

Online content

Any methods, additional references, Nature Portfolio reporting summaries, source data, extended data, supplementary information, acknowledgements, peer review information; details of author contributions and competing interests; and statements of data and code availability are available at <https://doi.org/10.1038/s41586-023-06527-1>.

- Einstein, A. Fundamental Ideas of the General Theory of Relativity and the Application of this Theory in Astronomy. In *Proc. Prussian Academy of Sciences* (1915).
- Dyson, F. W., Eddington, A. S. & Davidson, C. A determination of the deflection of light by the Sun's gravitational field, from observations made at the total eclipse of May 29, 1919. *Philos. Trans. Royal Soc. A* **220**, 291–333 (1920).
- Abbott, B. P. et al. (LIGO Scientific Collaboration and Virgo Collaboration) Observation of Gravitational Waves from a Binary Black Hole Merger. *Phys. Rev. Lett.* **116**, 061102 (2016).
- Dirac, P. A. M. The quantum theory of the electron. *Proc. R. Soc. A* **117**, 610–624 (1928).
- Anderson, C. D. The positive electron. *Phys. Rev.* **43**, 491–494 (1933).
- Nieto, M. M. & Goldman, T. The arguments against “antigravity” and the gravitational acceleration of antimatter. *Phys. Reports* **205**, 221–281 (1991).
- Hajdu Hajdukovic, D. S. Quantum vacuum and virtual gravitational dipoles: the solution to the dark energy problem? *Astrophys. Space Sci.* **339**, 1–5 (2012).
- Dimopoulos, C., Stamokostas, G. L., Gkouvelis, L. & Trigger, S. Hubble law and acceleration curve energies in a repulsive matter-antimatter galaxies simulation. *Astropart. Phys.* **147**, 102806 (2023).
- Villata, M. CPT symmetry and antimatter gravity in general relativity. *Eur. Phys. Lett.* **94**, 20001 (2011).
- Benoit-Lévy, A. & Chardin, G. Introducing the Dirac-Milne universe. *Astron. Astrophys.* **537**, A78 (2012).
- Touboul, P. et al. MICROSCOPE Mission: final results of the test of the equivalence principle. *Phys. Rev. Lett.* **129**, 121102 (2022).
- Witteborn, F. C. & Fairbank, W. M. Experiments to determine the force of gravity on single electrons and positrons. *Nature* **220**, 436 (1968).
- Andresen, G. B. et al. Evaporative cooling of antiprotons to cryogenic temperatures. *Phys. Rev. Lett.* **105**, 013003 (2010).
- Apostolakis, A. et al. Tests of the equivalence principle with neutral kaons. *Phys. Lett. B* **452**, 425 (1999).
- Borchert, M. J. et al. A 16-parts-per-trillion measurement of the antiproton-to-proton charge-mass ratio. *Nature* **601**, 53–57 (2022).

- Hughes, R. J. & Holzschneider, M. H. Constraints on the gravitational properties of antiprotons and positrons from cyclotron-frequency measurements. *Phys. Rev. Lett.* **66**, 854–857 (1991).
- Amoretti, M. et al. Production and detection of cold antihydrogen atoms. *Nature* **419**, 456–459 (2002).
- Andresen, G. B. et al. Trapped antihydrogen. *Nature* **468**, 673–676 (2010).
- Cesar, C. L. Trapping and spectroscopy of hydrogen. *Hyp. Interact.* **109**, 293–304 (1997).
- Gabrielse, G. Trapped antihydrogen for gravitation studies: is it possible? *Hyp. Interact.* **44**, 349–356 (1988).
- Amole, C. et al. Description and first application of a new technique to measure the gravitational mass of antihydrogen. *Nat. Commun.* **4**, 1785 (2013).
- Ahmadi, M. et al. Antihydrogen accumulation for fundamental symmetry tests. *Nat. Commun.* **8**, 681 (2017).
- Baker, C. J. et al. Laser cooling of antihydrogen atoms. *Nature* **592**, 35–42 (2021).
- Amole, C. et al. Resonant quantum transitions in trapped antihydrogen atoms. *Nature* **483**, 439–443 (2012).
- Ahmadi, M. et al. Observation of the hyperfine spectrum of antihydrogen. *Nature* **548**, 66–69 (2017).
- Ahmadi, M. et al. Observation of the 1S–2S transition in antihydrogen. *Nature* **541**, 506–510 (2017).
- Ahmadi, M. et al. Characterization of the 1S–2S transition in antihydrogen. *Nature* **557**, 71–75 (2018).
- Ahmadi, M. et al. Observation of the 1S–2P Lyman-alpha transition in antihydrogen. *Nature* **561**, 211–215 (2018).
- Ahmadi, M. et al. Investigation of the fine structure of antihydrogen. *Nature* **578**, 375–380 (2020).
- Maury, S. The antiproton decelerator: AD. *Hyp. Interact.* **109**, 43–52 (1997).
- Carli, C. et al. ELENA: bright perspectives for low energy antiproton physics. *Nuclear Physics News* **32**, 21–27 (2022).
- Surko, C. M., Greaves, R. G. & Charlton, M. Stored positrons for antihydrogen production. *Hyp. Interact.* **109**, 181–188 (1997).
- Baker, C. J. et al. Design and performance of a novel low energy multispecies beamline for an antihydrogen experiment. *Phys. Rev. Accel. Beams* **26**, 04010 (2023).
- Ahmadi, M. et al. Enhanced control and reproducibility of non-neutral plasmas. *Phys. Rev. Lett.* **120**, 025001 (2018).
- Amole, C. et al. In situ electromagnetic field diagnostics with an electron plasma in a Penning–Malmberg trap. *New J. Phys.* **16**, 013037 (2014).
- Zhong, M. et al. Axial to transverse energy mixing dynamics in octupole-based magnetostatic antihydrogen traps. *New J. Phys.* **20**, 053003 (2018).
- Ahmadi, M. et al. An improved limit on the charge of antihydrogen from stochastic acceleration. *Nature* **529**, 373–376 (2016).
- Hori, M. et al. Buffer-gas cooling of antiprotonic helium to 1.5 to 1.7 K, and antiproton-to-electron mass ratio. *Science* **354**, 610–614 (2016).
- Griffiths, D. J. & Schroeter, D. F. *Introduction to Quantum Mechanics* 3rd edn (Cambridge Univ. Press, 2018).
- Jonsell, S., Armour, E. A. G., Plummer, M., Liu, Y. & Todd, A. C. Helium–antihydrogen scattering at low energies. *New J. Phys.* **14**, 035013 (2012).
- Hodgkinson, D. *On the Dynamics of Adiabatically Cooled Antihydrogen in an Octupole-Based Ioffe-Pritchard Magnetic Trap*. PhD thesis, Univ. of Manchester (2022).
- Mansoulié, B. et al. Status of the GBAR experiment at CERN. *Hyp. Interact.* **240**, 11 (2019).
- Doser, M. et al. AEGIS at ELENA: outlook for physics with a pulsed cold antihydrogen beam. *Phil. Trans. Royal Soc. A* **376**, 20170274 (2018).
- Evetts, N. *Solid-state nuclear magnetic resonance magnetometry at low temperature with application to antimatter gravity experiments by ALPHA*. PhD thesis, Univ. of British Columbia (2021).
- Baker, C. J. et al. Sympathetic cooling of positrons to cryogenic temperatures for antihydrogen production. *Nat. Commun.* **12**, 6139 (2021).
- Hamilton, P. et al. Antimatter interferometry for gravity measurements. *Phys. Rev. Lett.* **112**, 121012 (2014).

Publisher's note Springer Nature remains neutral with regard to jurisdictional claims in published maps and institutional affiliations.



Open Access This article is licensed under a Creative Commons Attribution 4.0 International License, which permits use, sharing, adaptation, distribution and reproduction in any medium or format, as long as you give appropriate credit to the original author(s) and the source, provide a link to the Creative Commons licence, and indicate if changes were made. The images or other third party material in this article are included in the article's Creative Commons licence, unless indicated otherwise in a credit line to the material. If material is not included in the article's Creative Commons licence and your intended use is not permitted by statutory regulation or exceeds the permitted use, you will need to obtain permission directly from the copyright holder. To view a copy of this licence, visit <http://creativecommons.org/licenses/by/4.0/>.

© The Author(s) 2023